Supporting Information for "the Reaction Mechanism with Free Energy Barriers at Constant Potentials for the Oxygen Evolution Reaction at the IrO_2 (110) Surface"

Yuan Ping[1,2,3*], Robert J. Nielsen[1,2], William A. Goddard III[1,2*]

AUTHOR ADDRESS

[1]Joint Center for Artificial Photosynthesis, California Institute of Technology

[2] Materials and Process Simulation Center, California Institute of Technology

[3] Current address: The Department of Chemistry and Biochemistry, University of California, Santa Cruz

KEYWORDS: Density Functional Theory, Reaction Mechanism, Oxygen Evolution Reaction

Computational Details of DFT Calculations

We performed first principles calculations of the structural, electronic and vibrational properties of IrO_2 (110) surface using the open-source plane wave density functional theory (DFT) software Quantum Espresso[1]. The solvated calculations are performed using the open source DFT code, JDFTx[2], which implements several solvation models including SaLSA[3] and CANDLE[4]. We used the CANDLE solvation model, which improved the solvation energies of anions compared with SaLSA. Except the inclusion of solvation models, other numerical parameters including pseudopotentials, k points sampling, cell sizes, etc. are consistent between JDFTx and Quantum Espresso calculations.

We used GBRV ultrasoft pseudopotentials[5] at their recommended kinetic energy cutoffs of 20 and 100 Hartree for the wavefunctions and charge densities respectively. The Ir pseudopotential includes eight 5S,5P semicore electrons in the valence partition, whereas all other pseudopotentials (H and O) include valence electrons.

We employed the PBE generalized gradient approximation (GGA)[6] to the exchange correlation functional, with the DFT-D2 pair potential corrections[7] to account for the long-range London dispersion interactions, between small molecules (e.g., H_2O, O_2) and the IrO_2 surfaces.

We used Monkhorst-Pack k-point grids[8] for all the slab calculations: 5x5x1 for the (1x2) (110) IrO_2 surfaces. We used a smearing of 0.005 Hartree to resolve the Fermi surface of IrO_2 with Marzari-Vanderbilt[9] cold smearing, because IrO_2 is a metallic system.

We optimized the lattice constants and internal geometries of bulk IrO_2 from which we constructed slabs by appropriately repeating and terminating the bulk geometry. We then constrained the lattice vectors of the slabs at the two periodic directions and fully optimized all atomic positions self-consistently for each calculation in vacuum. Our slab model has five Ir-O tri-layers (see the O terminated IrO_2 (110) structure in Fig.S1).

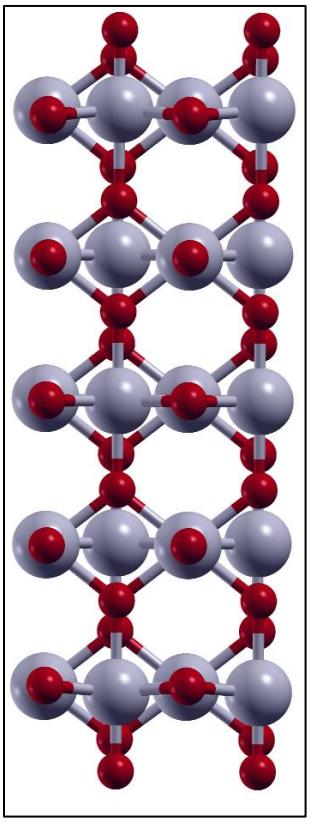

Figure S1. The atomic structure of O terminated (110) IrO_2 surface. Red balls: O; silver balls: Ir.

In all our slab models, we kept inversion symmetry to avoid the net dipoles in the supercell. We did self-consistent total energy calculations with implicit solvation models with and without geometry optimization and we

optimized values (<0.1 a.u. bond length). Then we did single-point total energy calculations using the CANDLE implicit solvation model after geometry optimization in vacuum. Our geometry optimization criterion converges the forces to be less than 10^{-4} Hartree/bohr on each atom.

The phonon vibrational frequencies are computed by Density Functional Perturbation Theory[10] (DFPT) for all the molecules and surface atoms (the atoms in the bulk region are frozen). We converged the self-consistency of phonon calculations to 10^{-14}. Unlike the finite difference method, DFPT does not need to displace the atoms, so that there is a no need to specify a step size. We found the ΔG with phonons from surface atoms changed less than 0.05 eV compared with the ones computed with phonon frequencies of the full slab. This greatly saved computational cost for the free energy calculations of surfaces.

The explicit constant electrochemical potential (μ_e) calculations using the implicit CANDLE solvation model were performed upon all reactions intermediates and transition states using JDFTx. All the numerical parameters and pseudopotentials are the same as the Quantum Espresso calculations. The ionic screening of net charges resulting from the constant μ_e condition was achieved with cation (0.1 M K^+) and anion (0.1 M F^-) components in the fluid model under the framework of joint density functional theory (JDFT). The algorithm employed by JDFTx variationally minimizes the grand free energy at the fixed electron chemical potential with respect to Kohn-Sham orbitals, fluid bound charges and an auxiliary Hamiltonian for the occupations[11].

For molecular calculations by Jaguar, all electrons are included for each H and O using the 6-311G**++ basis set for geometry optimization and vibration calculations. The zero-point energy, entropy and enthalpy due to translations, rotations and vibrations were calculated using the CPHF technique at the optimized geometry. The electronic energy of molecules used for computing barriers and reaction energies were obtained from JDFTx.

Other Geometries for a Layer of Explicit Water at (110) IrO_2 Surface

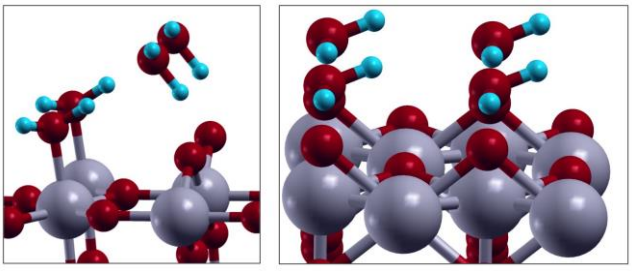

Figure S2. Other initial geometries (before geometry optimization) for IrO_2 (110) surface with a layer of explicit water molecules. Both geometries are unstable and H_2O spontaneously dissociated during the geometry optimization to form -OH terminated surface as shown in Figure 1 of the main text.

Other Geometries for the Initial States of TS-model3

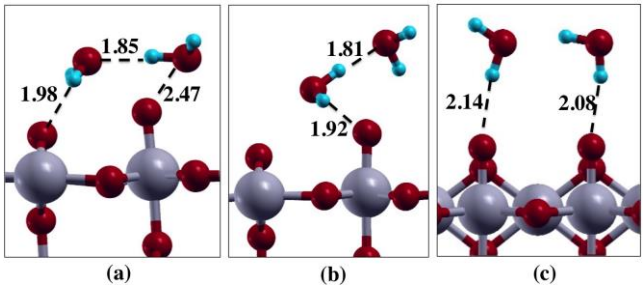

Figure S3. Different initial geometries for two H_2O molecules at IrO_2 (110) surface. Geometry (a) corresponds to the initial structure of TS-model3.

We considered three other water geometries at the IrO_2 (110) surface. All three geometries have forces optimized to their energy minimum. Geometry (a) has a total energy 0.5/0.7 eV lower than geometry (b)/(c). As a result, we chose geometry (a) for further transition state calculations as shown in Figure 6 in the main text.

Work Functions of IrO_2 Surface during Water Dissociation Reaction

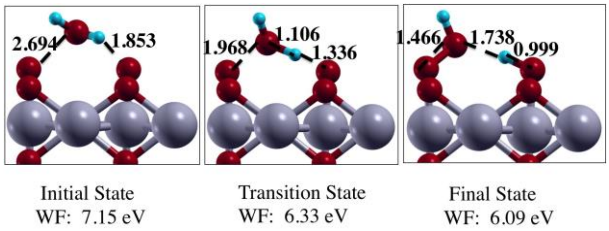

Figure S4. The work functions of (110) IrO_2 surface during water dissociation. The work function lowered (the Fermi level closer to the vacuum) by 1 eV during the water dissociation process at the surface at the constant charge condition. This indicates that the usual approach for QM, keeping the total charge fixed (where the work function of the surface is strongly affected by the water) may lead to increased errors compared to the constant potential (Grand Canonical) condition.

Reaction Energies and Barriers at Constant Potential and Constant Charge

In Table S1, we list the free energy comparison for the constant potential and constant charge calculations. Overall the difference of reaction energy at two conditions is ~ 0.05 eV and the difference in the energy barrier is ~0.1 eV. Most importantly, as discussed in the main manuscript, the steps that are electrochemically independent at

the constant charge become dependent on the electrochemical potentials at the constant potential condition, e.g. free energy difference of 1→ TS1 and 1→2.

elementary steps at U=1.53 eV vs NHE	Const. Charge ΔG[eV]	Const. Potential ΔG[eV]
1+H_2O→2	0.146	0.0668
1+H_2O→TS1	0.666	0.579
1+H^++e^-→1’	0.0918	0.134
1’+H_2O→TS1’	0.386	0.444
1’+H_2O→2’	-0.00104	0.106
2’→2+ H^++e^-	-0.173	-0.176
2→3+H^++e^-	-0.458	-0.503
3→4+H^++e^-	-0.0586	0.0213
4+ H_2O→TS2	0.470	0.560
4+H_2O→5+O_2	-0.390	-0.328
5→1’+H^++e^-	-0.302	-0.321
1’→1+H^++e^-	-0.137	-0.134
elementary steps at U=1.36 eV vs NHE		
1”→1’+H^++e^-	0.361	0.227
1’+ H_2O→TS1’	0.386	0.506
1’+ H_2O→2’	-0.00104	0.150
2’→2+H^++e^-	-0.00276	-0.00427
1’→1+H^++e^-	0.0782	-0.0189
1+ H_2O→TS1	0.666	0.622
1+ H_2O→2	0.146	0.127
2→3+H^++e^-	-0.254	-0.373
3→4+H^++e^-	0.194	0.186
4+H_2O→TS2	0.472	0.580
4+H_2O→5+O_2	-0.419	-0.297
5→1”	-0.398	-0.409

Table S1: free energy change of elementary steps (first column) at high potential (1.53 eV vs NHE) and low potential (1.36 eV vs NHE). The second column is the free energy change at the constant charge condition (see the main text); the third column is the free energy change at the constant potential condition, which are used for Fig. 2 and Fig. 5 in the main text.

Linearity of Reaction Barrier Free Energy as a Function of Applied Potential

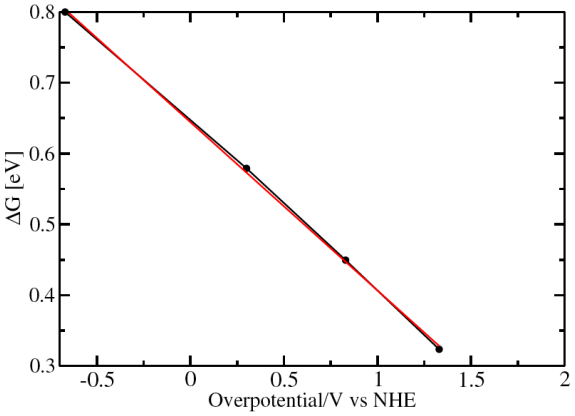

Figure S5. The reaction barrier of the water dissociation step (1->TS1) as a function of overpotential (relative to water oxidation potential (NHE+1.23 eV)) computed at the constant potential condition.

Fig. S5 shows the reaction barrier as a function of applied potential (x axis is the overpotential relative to water oxidation overpotential, NHE+1.23 eV). This shows that over a wide range of potential, the reaction barrier is linear with respect to the applied potential, similar to Figure 3 in the main text.

Surface Structure of the O-O Coupling Intermediate at the IrO_2 (110) Surface

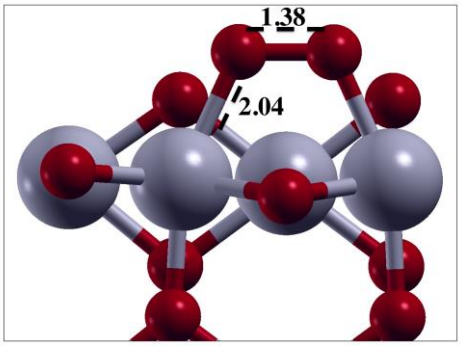

Figure S6. The O-O coupling structure at the IrO_2 (110) surface: red balls are O; silver balls are Ir. The bond lengths are given in the figure in Angstrom units.

An alternative pathway to form O-O bonds at the surface and generate O_2 molecules is through the couplings between two O atoms at the IrO_2 (110) surface as shown in Fig. S6. However, the formation of this reaction intermediates costs 0.62 eV free energy at U=1.53eV vs NHE, which is much less thermodynamically favorable than other intermediates in the water dissociation pathway. In addition, the formation of O_2 along the O-O coupling path will require breaking two Ir-O bonds instead of one in the water dissociation path.

CI-NEB Path of O_2 Removing from IrO_2 surface

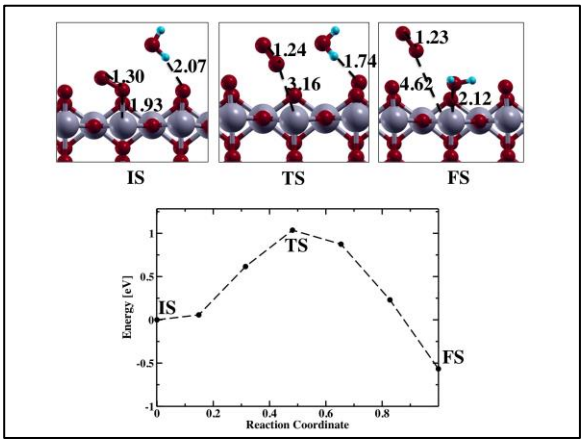

Figure S7. The NEB path for one O_2 to be substituted by one H_2O molecule showing only the electronic energies and the surface structures of initial state (IS), transition state (TS) and final state (FS). Including the effect of solvation, and the ZPE, enthalpy, entropy contributions to the free energy, we obtain a transition state barrier of 0.39 eV (assuming that the translational and rotational enthalpy and entropy of O_2 is from the gas phase) and we obtain 0.56 eV (if we consider the translational and rotational enthalpy and entropy of O_2 is from 1M O_2 in liquid H_2O) at U=1.53 eV vs NHE.

Details of the Micro-kinetic Model

In our Micro-kinetic model, we consider reactions 1+H_2O->2 and 1'+H_2O->2' are competing reactions as discussed in the main text, and we assume that they are the rate-determining steps. We did not consider the back reactions from 2->1+H_2O and 2'->1'+H_2O, because reactions 2->3+H^++e^- and 2'->2+H^++e^- are thermodynamically downhill and barrierless, therefore most species at intermediates 2 and 2' will quickly convert to intermediate 3. We found that water can only dissociate at surface structure 1 (O terminated surface) and 1' (25% -OH terminated surface) in Fig.2. Therefore, the reaction rate can be written as:

$$R = k_{25}[C_{25}] + k_0[C_0] \quad (1)$$

$$k_{25} = \frac{kT}{h} exp(-\frac{G_{25}(\eta)}{kT}) \quad (2)$$

R is the reaction rate, C_{25} and C_0 are the concentrations of active sites at 25% OH terminated surface and 0% OH terminated surface (O terminated surface). k_{25} and k_0 are the reaction rates at the two corresponding surfaces. This can be computed from Eq.2, based on classical transition state theory. G_{25} is the reaction barrier of water dissociation at 25% -OH terminated surface. η is the overpotential for oxidizing H_2O (the potential relative to NHE+1.23 eV).

Next we can rewrite C_{25} and C_0 based on the total catalytic site balance:

$$[M_0] = [C_0] + [C_{25}] + [C_{50}] + [C_{75}] + [C_{100}] \quad (3)$$

where the total active site concentration $[M_0]$ is the sum of the active site concentration at all possible surfaces with various OH coverages. Then we can relate $[C_0]$ and $[C_{25}]$ with equilibrium constants:

$$K_{025} = {}^{C_{25}}/_{C_0} \quad (4)$$

$$K_{025} = exp(-\frac{G_{025}(\eta)}{kT}) \quad (5)$$

where G_{025} is the reaction energy for protonating the O terminated surface to the 25% -OH covered surface. Then Eq. (3) can be rewritten by the equilibrium constants between $[C_0]$ and active site concentrations at other surfaces (similar to Eq.4), leading to:

$$[C_0] = \frac{[M_0]}{1+K_{025}+K_{050}+K_{075}+K_{0100}} \quad (6)$$

Combining Eq. 4 and Eq. 6 we obtain:

$$[C_{25}] = \frac{K_{025}[M_0]}{1+K_{025}+K_{050}+K_{075}+K_{0100}} \quad (7)$$

As a result, combining Eq. 1, Eq. 6 and Eq. 7, leads to:

$$R = \frac{[M_0]k_0 + [M_0]k_{25}K_{025}}{1 + K_{025} + K_{050} + K_{075} + K_{0100}} \quad (8)$$

At the end we can compute R by substituting k_0, k_{25}, K_{025}, K_{050}, K_{075}, K_{0100} with Eq. 2 and Eq. 5 using corresponding reaction barriers.

O_2 Binding Energy at Ir by PBE and B3LYP levels of DFT

It is highly likely that DFT using the PBE functional overbinds O_2, which would lead to an overestimate for the reaction barrier of evolving O_2 from the IrO_2 surface. To test the accuracy, we used a IrO_2 cluster model (analogous to our surface reactions) as shown in Fig. S8. We calculate that removing O_2 and adding H_2O onto Ir atom in Fig. S8, leads to a binding energy 10 kcal/mol (0.43 eV) higher for PBE-D3 compared with B3LYP-D3 (which generally yields more accurate reaction energies). This overbinding of O_2 by semi-local functionals has also been discussed in Ref.10.

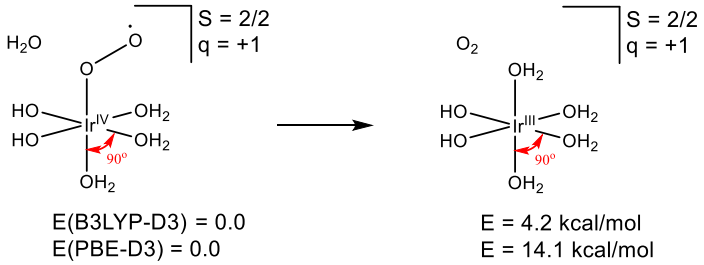

Figure S8. Using this IrO_2 cluster model, we calculated the reaction energy of substituting O_2 by H_2O on Ir atom with both the B3LYP-D3 and PBE-D3 functionals. The reaction energy using PBE-D3 is 9.9 kcal/mol higher than for B3LYP-D3.

References

1. Giannozzi, P. et al. *J Phys-Condens Mat* 2009, *21*, 295502. Giannozzi, P.; Baroni, S.; Bonini, N.; Calandra, M.; Car, R.; Cavazzoni, C.; Ceresoli, D.; Chiarotti, G. L.; Cococcioni, M.; Dabo, I.; Dal Corso, A.; de Gironcoli, S.; Fabris, S.; Fratesi, G.; Gebauer, R.; Gerstmann, U.; Gougoussis, C.; Kokalj, A.; Lazzeri, M.; Martin-Samos, L.; Marzari, N.; Mauri, F.; Mazzarello, R.; Paolini, S.; Pasquarello, A.; Paulatto, L.; Sbraccia, C.; Scandolo, S.; Sclauzero, G.; Seitsonen, A. P.; Smogunov, A.; Umari, P.; Wentzcovitch, R. M. J. Phys.: Condens. Matter (2009), **21**, 395502.
2. Letchworth-Weaver, K.; Arias, T. A. *Phys Rev B* (2012), **86**, 075140. Gunceler, D.; Letchworth-Weaver, K.; Sundararaman, R.; Schwarz, K. A.; Arias, T. A. *Model Simul Mater Sc* (2013), **21**, 074005.
3. Sundararaman R.; Schwarz, K.; Letchworth-Weaver, K. and Arias, T. A. J. Chem. Phys. (2015), **142**, 054102.
4. Sundararaman, R.; Goddard, W. A. *J Chem Phys* (2015), **142**, 064107.
5. Garrity, K. F.; Bennett, J. W.; Rabe, K. M.; Vanderbilt, D. *Comp Mater Sci* (2014), **81**, 446.
6. Perdew, J. P.; Kieron, B.; Matthias, E. *Phys. Rev. Lett*. (1996), **66**, 3865.
7. Grimme, S. *J Comput Chem* (2006), **27**, 1787.
8. Monkhorst, H. J. and Pack, J. D. *Phys. Rev. B*, (1976), **13**, 5188.
9. Marzari, N.; Vanderbilt, D.; De Vita, A.; Payne, M. C. *Phys. Rev. Lett*. (1999), **82**, 3296-3299.
10. Baroni, S.; de Gironcoli, S.; Dal Corso, A.; Giannozzi, P. *Rev Mod Phys* (2001**)**, **73**, 515.
11. R. Sundararaman, W. A. Goddard., T. A. Arias, *under preparation*, (2016).
12. M. Liao, M. Huang, J. Watts, *Mol. Phys.* (2011), **109**, (16):2035-2048.